Soft Matter

RSC Publishing

PAPER

View Article Online
View Journal | View Issue

Cite this: *Soft Matter*, 2013, **9**, 3798

Understanding the reinforcing behavior of expanded clay particles in natural rubber compounds†

Sandip Rooj,[ab] Amit Das,[a] Klaus Werner Stöckelhuber,[a] De-Yi Wang,[a] Vassilios Galiatsatos[a] and Gert Heinrich*[ab]

Received 16th July 2012
Accepted 18th January 2013

DOI: 10.1039/c3sm27519a

www.rsc.org/softmatter

We report the unusual mechanical percolation behavior of expanded clay nanoparticles in a natural rubber (NR) matrix. This phenomenon is discussed in terms of fractal dimensions of the nanoparticle cluster. Highly exfoliated structures of nanoparticles in NR are obtained by a process we call the 'propping-open approach'. The impact of filler dispersion and rubber–filler interactions on the viscoelastic behavior of NR–clay nanocomposites is systematically investigated. We observe non-linear viscoelastic behavior (Payne effect) at very low nanoparticle concentrations which we attribute to the formation of a network-like structure of the exfoliated clay particles. We rely on the Kraus and Maier–Göritz models to interpret such nonlinear viscoelastic behavior. We find that the chain mobility of the NR is greatly reduced based on the viscoelastic master curves. The value of the mechanical percolation threshold (φ_p) and the fractal nature of nanoparticle clusters are determined through an analysis of the experimental data based on a theory put forward by Huber and Vilgis. The nature of rubber–filler interactions is further understood from swelling experiments utilizing the Kraus and Cunneen–Russell equations.

1 Introduction

The presence of strong electrostatic forces between clay layers[1] limits the successful preparation of clay–rubber nanocomposites, especially in the case of non-polar rubbers like natural rubber (NR). This challenge persists even after the organic modification of clay.[2,3] To successfully overcome this problem, a new approach called the "propping-open" approach has been adopted and reported by us.[4,5] We relied on an idea first investigated by Brindley and Ray in 1964 and extended it to the field of polymer nanocomposites.[6] This process utilizes the stepwise expansion of the interlayer space of Ca^{2+}-montmorillonite (MMT) clay by swelling with several solvents. In our reported work, quaternary ammonium modified MMT (abbreviated as OMT) was treated with long chain fatty acids (*e.g.* docosanoic acid) and this organic acid expanded the interlayer space between the clay layers and ultimately aided the dispersion. The efficacy of fatty acids with longer alkyl chain length on the exfoliation of MMT in non-polar rubber like NR has also been reported by us.[4,5] Among the fatty acids with different chain lengths studied, the fatty acid containing 22 carbon atoms (docosanoic acid) yields the most interlayer space. For that reason it is selected for the work reported here.

Polymer-layered silicate nanocomposites have attracted a great interest for the last few years in the field of polymer science and technology since their invention by the Toyota research group.[7] In general, nano-sized particles offer the same level of reinforcement as carbon black and silica but at relatively lower loading.[8–10] The mechanical properties of conventional rubber composites depend mostly on the degree of the dispersion of fillers,[11] the structure of the fillers,[12] and rubber–filler and filler–filler interactions.[13,14] Using the 'cluster–cluster aggregation' model (CCA), Klüppel *et al.*[15] showed that the storage modulus of the filler network is directly related to $\varphi^{3.5}$ (φ stands for the filler volume fraction) where the exponent "3.5" reflects the characteristic structure of the fractal heterogeneity of the filler. Therefore, the reinforcement effect is mostly attributed to the development of a percolating network of the filler particles. However, many studies have shown that the addition of fillers within a polymer matrix can lead to the formation of a modified polymer layer in the vicinity of the filler surface, the so-called interphase or bound rubber.[16,17] The presence of such an additional phase could affect the overall mechanical properties of the rubber composites. Immobilization of ethylene propylene rubber (EPDM) chains on the surface of carbon black and network structure in the rubber matrix of filled EPDM rubbers were studied and reported by Litvinov *et al.* using low-field proton NMR experiments.[16] The thickness of the immobilized EPDM–carbon black interfacial layer was estimated to be ≥0.6 nm.[16] Papon *et al.* developed a microscopic model and pointed out that strong reinforcement is obtained when glassy layers between fillers overlap.[18] Sternstein and

[a]*Leibniz-Institut für Polymerforschung Dresden e. V., Hohe Straße 6, D-01069 Dresden, Germany. E-mail: gheinrich@ipfdd.de*

[b]*Technische Universität Dresden, Institut für Werkstoffwissenschaft, D-01069 Dresden, Germany*

† Electronic supplementary information (ESI) available. See DOI: 10.1039/c3sm27519a

Zhu[19] have established experimentally that the principal underlying mechanism for reinforcement and nonlinear viscoelastic behavior is attributed to filler–matrix interactions, for example trapped entanglements, rather than filler agglomeration.

This investigation is focused on the relationship between filler dispersion and the viscoelastic behavior of NR filled with layered silicate. Morphological characterization by transmission electron microscopy (TEM) and wide angle X-ray diffraction pattern (WAXD) is complemented by a quantitative analysis of mechanical properties. We rely on theoretical models such as those of Guth–Smallwood[20] and Halpin–Tsai[21] to understand the reinforcement behavior of the nanoparticle filled rubber matrix. To delineate the filler–filler interaction, especially at very low filler loading, a detailed analysis of strain sweep measurements is presented by employing concepts put forth by Kraus[22] and Maier–Göritz.[23] Finally, we analyze our data by using a theory developed by Huber and Vilgis[24] to determine and understand the fractal dimension of the nanoparticle clusters.

2 Experimental

2.1 Materials

Natural rubber (NR) was Standard Malaysian Rubber (SMR). Stearic acid was purchased from ACROS Organics, Geel, Belgium, with 97% purity. The vulcanizing accelerator *N-tert*-butylbenzothiazolesulfenamide (TBBS) was kindly provided by Rhein Chemie Rheinau, Mannheim, Germany. Sulphur (S) and zinc oxide (ZnO) used in this study were of industrial grade. Organomontmorillonite (OMT) was supplied by Süd-Chemie AG (now Rockwood Additives), Moosburg, Germany. The organic modifier was in this case distearyl dimethylammonium chloride (QUAT). The specific gravity of this OMT was 1.8 g cm^{-3}. Docosanoic acid (C22) was procured from ACROS Organics, Geel, Belgium.

2.2 Preparation of expanded clay (EMT)

In order to increase the interlayer space, intercalation of fatty acids was performed in an internal mixer (Haake Rheomix, Thermo Electron GmbH, Karlsruhe). For this purpose, a mixture of OMT and fatty acid (1 : 1 by mass) was mixed using a fixed rotor speed of 50 r.p.m. and a temperature of 100 °C. These blends were mixed for 20 minutes. The blend was then cooled to room temperature and it was grinded subsequently. The successful intercalation of docosanoic acid was confirmed by X-ray diffraction analysis. The resulting product is called expanded organo-montmorillonite (abbreviated as EMT).[4,5]

2.3 Preparation of EMT and the NR nanocomposites

The formulation of NR compounds in parts per hundred of rubber (phr) is as follows: zinc oxide ZnO (5), stearic acid (2), sulphur (1.4), TBBS (1.4), OMT (10) and EMT (2 to 10 phr). Details of this formulation are summarized in Table S1 in the ESI.† Mixing of NR with EMT was performed with an open two-roll mixing mill (Polymix 110L, size: 203 mm × 102 mm, Servitec GmbH, Wustermark, Germany) at 90 °C. This temperature was selected to ensure complete melting of fatty acids during mixing. NR was first masticated and mixed with ZnO. EMT was then incorporated. Finally, this step was continued for 5 min keeping ~0.15 mm nip gap between the rolls. The compounded rubber was then mixed with the TBBS and S. For control batches the mixing sequence was first zinc oxide, followed by stearic acid, OMT, accelerator and finally S. The total mixing and compounding cycle was 20 min for each blend. The stocks were cured under pressure at 150 °C to 2 mm sheets using the optimum cure time (t_{90}) previously determined from a vulcameter (Scarabaeus, Langgöns, Germany).

2.4 Characterization techniques

The state of dispersion of the clay particles in the nanocomposites was investigated using transmission electron microscopy (JEM 2010). The ultra-thin sections of the samples were prepared by ultramicrotomy (Leica Ultracut UCT) at −120 °C. Dynamic mechanical analysis was performed on strips with 10 mm width using a dynamic mechanical thermal spectrometer (Gabo Qualimeter, Ahlden, Germany, model Eplexor-2000N) in the tension mode. The isochronal frequency employed was 10 Hz and the heating rate was 2 °C min^{-1} with a dynamic load at 0.5% strain and a static load at 1% strain. Amplitude sweep measurements were performed on the same Eplexor 2000 N in the tension mode at room temperature, at a constant frequency of 10 Hz, static load at 60% pre-strain and dynamic load 0.01–30%. Frequency master curves were made by using the time temperature superposition principle (TTS), after measuring a combined temperature frequency sweep at temperatures from 20 °C to 100 °C and frequencies from 0.5 Hz to 50 Hz. For creating the master curves, the instrument software (Eplexor version 8.374g from Gabo, Ahlden, Germany) was used. Tensile tests of cured samples were carried out using a material testing machine (Zwick 1456, model 1456, Z010, Ulm, Germany) with a crosshead speed of 200 mm min^{-1} (ISO 527). The differential scanning calorimeter (DSC) measurements were performed on a Q1000 (TA Instruments, New Castle, USA) coupled with an auto-sampler in the temperature range of −80 °C to 210 °C for all the samples at a scanning rate of 10 K min^{-1} under a nitrogen atmosphere.

Swelling experiments were performed according to ASTM D 6814-02. Previously weighed samples were allowed to swell in toluene at 25 °C for 24 h, the equilibrium swelling time (which was determined from a plot of mass uptake against time). The test pieces were then taken out, weighed and dried to a constant weight in a vacuum oven at 50 °C for 12 h. The volume fraction of the rubber in the swollen gel (V_r) was determined on the basis of a simple additive rule of volumes as follows (eqn (1)):

$$V_r = \frac{(D - FH)/\rho_r}{(D - FH)/\rho_r + A_o/\rho_s} \quad (1)$$

where H = weight of the test specimen, D = weight of the deswollen test specimen, F = weight fraction of the insoluble components, A_o = weight of the absorbed solvent, ρ_r = density of the rubber, and ρ_s = density of the solvent.

3 Results and discussion

3.1 Modulated differential scanning calorimetry (MDSC)

Fig. 1 shows DSC thermograms of NR and nanocomposites with various amounts of filler loading. It is observed that the T_g of pure NR gum compound is ~−62 °C. In the present study, the results are analyzed in terms of T_g and a change in heat capacity (ΔC_p) at constant pressure at T_g. In principle, ΔC_p is related to the fraction of the polymer participating at the glass transition and is proportional to the number of internal degrees of freedom of molecular motion. It is shown from Table 1 that T_g does not change with composition. However, ΔC_p at T_g, normalized to the fraction of amorphous polymer, systematically decreases with increasing filler content. As more and more EMT is added into the nanocomposite system, a higher fraction of polymer chains is confined between the clay layers. This would further decrease the degree of freedom of the polymer chain segments, thus causing ΔC_p values to decrease with increasing EMT content. Similar results have been obtained with other polymer nanocomposites.[25] Therefore the values of ΔC_p depend on the amount of EMT in the polymer matrix and can thus be conveniently utilized to indicate the approximate inherent interfacial interaction between the polymer and the filler surface. The fraction of immobilized polymer can then be calculated by eqn (2) given below:[25]

$$x_{im} = 1 - \frac{\Delta C_p}{\Delta C_{p0}(1 - w)} \quad (2)$$

where ΔC_{p0} is the heat capacity increment of the neat rubber and w is the weight fraction of EMT.

The values of X_{im} thus obtained are depicted in Table 1. For the NR–EMT nanocomposites, they range from 10 to 14% and they are increasing with increasing EMT content. Therefore, the increased amount of adsorbed rubber chains on the filler surface is attributed to stronger rubber–filler interactions.

3.2 Morphology of nanocomposites: TEM

TEM investigation was carried out to examine directly the intercalation of rubber chains and the dispersion of the EMT in the NR matrix. Fig. 2 shows the TEM micrographs of NR nanocomposites with both OMT and EMT. The dark lines and areas are EMT layers and aggregates, and the light area shows the rubber matrix. The thickness of most EMT tactoids is 7–8 nm and the length is about 80–200 nm and these numbers are independent of the EMT loading. However, large agglomerates of clay particles are observed in the case of OMT filled NR composites. Therefore, a dramatic improvement in the dispersion of clay nanoparticles is observed when EMT is used.[5] At lower magnification, the EMT appears to be well dispersed in the rubber matrix. One can observe the presence of some individual silicate layers throughout the rubber matrix at high magnification and a few stacks of EMT particles are visible indicating a partially to highly exfoliated morphology of EMT.

Table 1 Different parameters obtained from MDSC

Sample	T_g (°C)	ΔC_p (J g^{-1} K^{-1})	X_{im}
Gum	−62	0.44	—
EMT-2	−62	0.39	0.10
EMT-4	−62	0.38	0.11
EMT-6	−62	0.38	0.11
EMT-10	−63	0.36	0.14
OMT-10	−62	0.40	0.04

3.3 Reinforcing mechanism and mechanical modeling of modulus

To further understand the reinforcing mechanism of the filled elastomer matrix, tensile properties of various systems were analyzed in detail utilizing particulate composite reinforcement models.[26] Many empirical or semi empirical equations have been proposed to predict the so-called "hydrodynamic amplification" of the equilibrium modulus of particulate–polymer

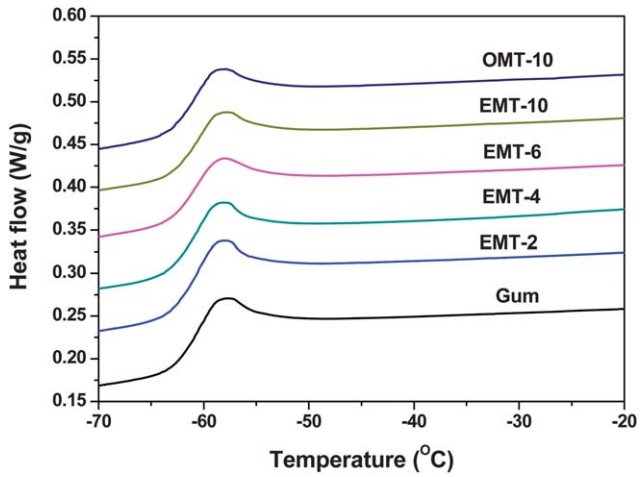

Fig. 1 DSC thermograms of different NR–EMT nanocomposites.

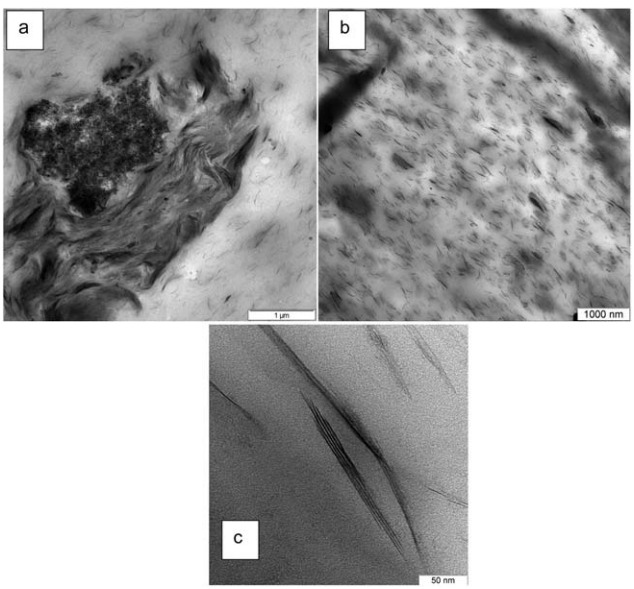

Fig. 2 Different TEM images of NR nanocomposites with (a) 10 phr of OMT, (b) 10 phr of EMT at low magnification and (c) 10 phr of EMT at high magnification.

composites. If the filler particles are sufficiently rigid, *i.e.* their elastic modulus is much larger than that of the rubber ($E_{filler}/E_m \gg 1$), then the large majority of the elastic energy will be stored in the rubber and one obtains[27]

$$E_\delta = \frac{E_c}{E_m} = 1 + 2.5\varphi + \alpha\varphi^2 \quad (3)$$

E_δ is known as modulus enhancement, E_c and E_m are tensile moduli of the nanocomposite and the pure matrix, respectively, and φ is the volume fraction of filler particles dispersed in the rubber matrix. The values of E_m and E_c are obtained from the linear region of the stress–strain graphs. The parameter α in the second order term varies according to the different approaches. Guth and Gold[20] report $\alpha = 14.1$, whereas Batchelor and Green[28] derived $\alpha = 5.2$ for the shear modulus of a filled elastic solid with a predicted error in the φ^2 term of $\pm 0.3\varphi^2$. A similar value of $\alpha = 5.0$ was found by Chen and Acrivos.[29] However, it was also found that for a higher volume fraction of the filler (*e.g.* 10 vol %), the reinforcing factor increases more rapidly compared to the values calculated by eqn (4).[30] This could be attributed to the formation of a network structure by the spherical filler. To circumvent that issue, Guth developed the following equation. In particular Guth introduced a parameter f which is known as shape factor (defined as the ratio of length to thickness) in order to explain stiffening caused by a chain-like structure or non-spherical particles:

$$E_\delta = 1 + 0.67f\varphi + 1.62f^2\varphi^2 \quad (4)$$

As in the present case the particles have a plate like geometry (non-spherical) with high aspect ratio, we consider the above equations to acquire a rough understanding of the reinforcement effect by the silicate nanoparticles.

The Halpin–Tsai eqn (21) also has served as a popular model since it can be accurately employed to quantify the reinforcement of the filler in nanocomposites. The elastic modulus of the nanocomposites filled with fully aligned fibrous reinforcing particulates is given by Halpin–Tsai[21] as follows:

$$E_\delta = \frac{E_c}{E_m} = \frac{1 + 2f\eta\varphi}{1 - \eta\varphi} \quad (5)$$

where f is the aspect ratio, $\eta = \dfrac{E_{filler}/E_m - 1}{E_{filler}/E_m - 2f}$ and E_{filler} is the Young modulus of the filler.

In the dilute stiff fiber limit ($\varphi \ll 1$ and $E_{filler}/E_m \gg 1$) the above equation[31] can be expressed as

$$E_\delta = 1 + 2f\left(\frac{E_f/E_m}{E_f/E_m - 2f}\right)\varphi \quad (6)$$

According to Schaefer and Justice,[31] eqn (6) becomes independent of fiber elastic properties especially in the case of short fiber limit ($2f \ll E_{filler}/E_m$). Therefore, eqn (6) reduces to

$$E_\delta = 1 + 2f\varphi \quad (7)$$

If the fibers are not aligned, a parameter known as the angular factor should be included in eqn (7), giving

$$E_\delta = 1 + 2fC_a\varphi \quad (8)$$

For clay particles the value of C_a is nearly 0.5. Therefore, eqn (8) is reduced to

$$E_\delta = 1 + f\varphi \quad (9)$$

In this study, we rely on the models above to fit the mechanical properties of the NR–EMT nanocomposites. The aspect ratio (f), which is a fitting parameter, was obtained according to the best fit and was determined to be 32 and 100, respectively. In general, the average aspect ratio of the individual MMT nanoparticle is in the range of 100 to 150.[32] This finding is in agreement with previous investigations.[30,32]

The aim of this section is to select a few of the most widely used models from the literature[30,32] and compare their usefulness in predicting the modulus of NR reinforced with EMT. The reinforcement factor (E_c/E_m) is plotted as a function of the EMT volume fraction (φ) in Fig. 3. It is interesting to note that the reinforcement factor is increased with an increase of the filler volume fraction. The Guth–Smallwood model deviates from the experimental results, but the Halpin–Tsai model fits well within the volume fraction range investigated. Although it is not discussed in detail here, one might assume that larger deviations of Guth–Smallwood from experimental data could be traced back to a violation of the above mentioned assumptions behind eqn (3) and (4), *i.e.* a certain amount of energy could be stored in bendable clay particles. This is different from carbon black or silica particles and might be especially important in the case of EMT particles.

The aspect ratio is calculated from TEM image analysis too using TEM micrographs, which is rather a direct measurement of some parameters like length and thickness of the filler particles. Details of this image analysis are given in the ESI (Fig. S1†). The value of aspect ratio obtained from this image analysis is very low compared to the aspect ratio obtained from Halpin–Tsai modeling. The aspect ratio calculated from TEM image analysis again underestimates the mechanical properties. A similar observation was reported by Schafer and Justice.[31] The aspect ratio calculated from ultra-small-angle X-ray scattering by

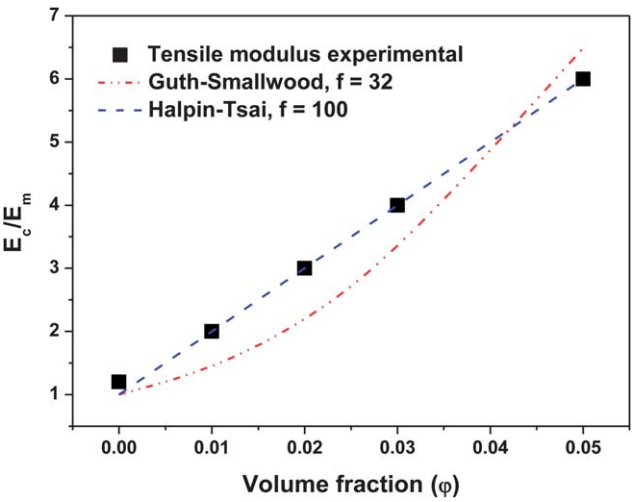

Fig. 3 Plots of tensile modulus using different models.

Schafer and Justice[31] was also lower compared to the value of aspect ratio obtained from Halpin–Tsai modeling in the case of polyamide-layered silicate composites. We also believe that the aspect ratio estimated by this TEM image analysis is lower than the real average aspect ratio of the clay platelets, which is attributed to several problems like focusing errors and disorientation, which can increase their apparent thickness, and low contrast preventing identification of some platelets.

3.4 Viscoelasticity and non-linear viscoelastic behavior

Strain sweep measurements were performed in order to investigate the polymer–filler and filler–filler interactions. The results demonstrate the qualitative features usually attributed to the Payne effect. The effect of the dynamic strain amplitude on the E' and E'' at different EMT loading is documented in Fig. 4. The storage modulus is at the highest at small amplitude (referred to as E'_0) and gradually decreases to a lower value (referred to as E'_∞). The magnitude of the Payne effect ($E'_0 - E'_\infty$) is increased with increasing EMT content. At low EMT loading (for instance 2 phr), the observed variation in the amplitude of the Payne effect is weak. However, as the EMT concentration increases, pronounced variation is observed.

We attribute this behavior to the breakdown of the filler–filler networks at higher strains. When comparing the magnitude of the Payne effect (for equivalent volume fractions) 10 phr OMT has an extremely low value compared to that of 10 phr EMT. It should be noted here that the network structure of the exfoliated particles was not clearly observed in the TEM images but an indication of the filler–filler network has been observed in the strain sweep experiments (see Table 2). Filler–filler networks can be developed with the same volume fraction of fillers when they break down into a large number of particles.

Several models are available for the interpretation of strain-sweep measurements.[33,34] To parameterize the amplitude-sweep curves, we employed the phenomenological but quantitative Kraus model.[22] This approach is based on the assumption of an agglomeration/deagglomeration mechanism of filler agglomerates:

$$\frac{E'(\gamma) - E'_\infty}{E'_0 - E'_\infty} = \frac{1}{1 + \left(\frac{\gamma_0}{\gamma_c}\right)^{2m}} \quad (10)$$

Table 2 Parameters obtained from strain sweep measurements

Sample	E'_0 (MPa)	E'_∞ (MPa)	$E'_0 - E'_\infty$ (MPa)
EMT-2	2.58	1.82	0.76
EMT-4	3.67	1.86	1.81
EMT-6	4.87	1.91	2.96
EMT-10	7.01	2.00	5.01
OMT-10	3.6	2.00	1.60

where E'_∞ is equal to $E'(\gamma)$ for very large strain, E'_0 is equal to $E'(\gamma)$ for very low strain, γ_c is a characteristic shear strain amplitude known as critical strain, $E'_0 - E'_\infty$ is reduced to half of its zero-strain value, and the parameter m gives the shear strain sensitivity of the mechanism of filler–filler contact breakage; it defines the shape of the $E'(\gamma)$ curves.

The values of E'' are also fitted according to the Kraus model. In this case the expression of E'' is given by eqn (11):

$$\frac{E''(\gamma) - E''_\infty}{E''_m - E''_\infty} = 2\frac{\left(\frac{\gamma_0}{\gamma_c}\right)^m}{1 + \left(\frac{\gamma_0}{\gamma_c}\right)^{2m}} \quad (11)$$

where E''_m is the maximum loss modulus at $\gamma_0 = \gamma_c$.

It is clear from Fig. 5b that the Kraus model cannot match the asymmetric shape of E'' *vs.* strain (γ) data. A further comparison between experimental and theoretical data obtained with the Kraus model is proposed in Fig. 5a and b. Fitted values are given in Table S2 and Table S3† in the supporting Information. The Kraus model does describe the variation of $E' = f(\gamma)$ for EMT concentrations higher than 4–6 phr (corresponding to the percolation threshold concentration). We cannot fit the Kraus model below this EMT concentration. This result is consistent with the assumptions of this model. However, differences can be observed between experimental and theoretical values of the loss modulus E'' *versus* strain amplitude (Fig. 5b). Fitted values are shifted toward higher deformations when compared with experimental variations. There is published work that reports similar observations.[33,34] The reason behind this is still under debate.

In order to better understand the influence of the matrix–filler interaction on the viscoelastic properties of

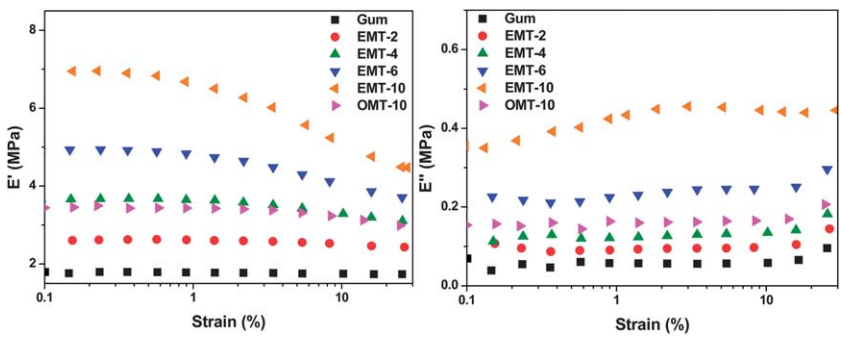

Fig. 4 Dependence of amplitude sweep on (a) E' and (b) E'' of different NR–clay nanocomposites.

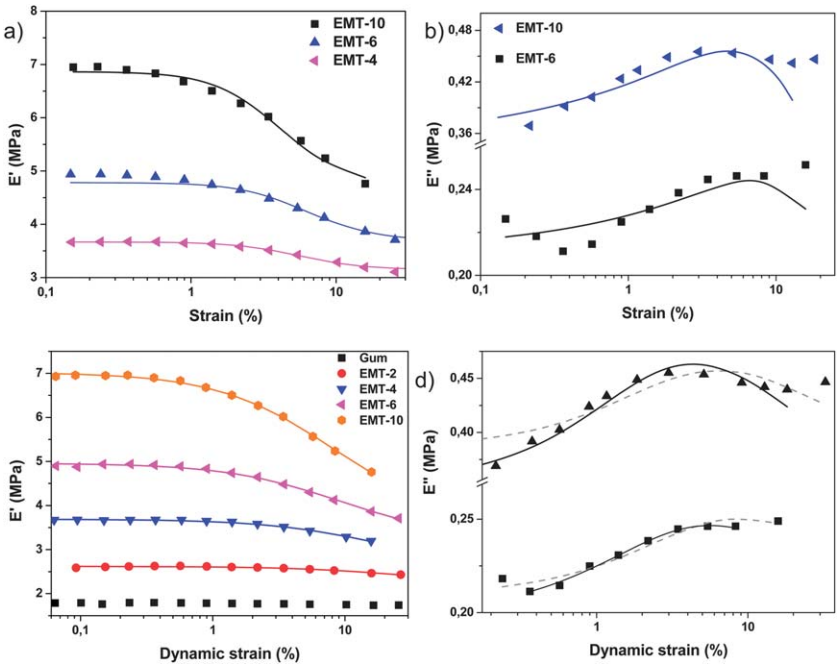

Fig. 5 (a) E' values fitted according to the Kraus model. (b) E'' values fitted according to the Kraus model. (c) E' values fitted according to the Maier–Göritz model. (d) Dashed lines and solid lines represent the calculated E'' using the Maier–Göritz and modified Maier–Göritz models for EMT-10 (◀) and EMT-6 (■).

nanocomposites, we employed the Maier–Göritz model. This model offers a molecular interpretation of the Payne effect based on the rubber–filler interactions.[23] In general, the adsorption process occurs at the filler surface when the filler is mixed with rubber. The formation of the first rubber–filler inter–link on an interaction site present on the filler surface favors the formation of several other links on neighboring interaction sites. The first rubber chain is adsorbed firmly onto the filler surface and forms the so-called 'stable bonds'. The chains arriving later at the filler surface have fewer chances to generate bonds with the filler. Therefore those chains are only able to form 'unstable bonds' with the filler surface. Those unstable bonds are very fragile and are prone to break, when mechanical stress is applied or if the temperature is raised.

According to this model, the evolution of storage modulus with strain is given by eqn (12):

$$E'(\gamma) = E'_{st} + E'_{i}\frac{1}{(1+c\gamma)} \quad (12)$$

E'_{st} is the value of storage modulus at high deformations (referred to as E'_{∞}) and E'_{i} represents the amplitude of the Payne effect: $E'_{i} = E'_{0} - E'_{st}$ where 'c' defines the position of the E' curve on the strain axis. Generally, the expression of $E'(\gamma)$ is similar to that of the original Kraus model,[22] which uses filler networking as the reason for the Payne effect. In the equation of Kraus[22] an additional slope exponent m appears, *i.e.* $E'(\gamma) \sim (1 + c\gamma)^{-2m}$

However, many authors[33] have shown that this exponent is around 1/2, *i.e.* $2m = 1$, as indeed is assumed in the Maier–Göritz model.[23]

The loss modulus E'' variation *versus* strain amplitude is given by eqn (13):

$$E''(\gamma) = E''_{st} + E''_{i}\frac{c\gamma}{(1+c\gamma)^2} \quad (13)$$

E''_{st} is the E'' value when γ has very low or very high values, E''_{i} gives the variation amplitude of E'' and 'c' defines the position of the E'', maximum on the strain axis.

A good agreement is observed between experimental and fitted values of E'. This holds regardless of the volume fraction of EMT (Fig. 5c). It is also interesting to note that the Maier–Göritz model is able to fit the non-linear viscoelastic behavior of the low EMT loaded sample (2 phr) reasonably well compared to the Kraus model. EMT favors the intercalation of a large number of rubber chains in the clay nanogalleries. This is attributed to the high interlayer spacing of EMT which further enhances the rubber–filler interactions.

However, a small discrepancy is detected in the case of E'' when fitted against dynamic strain amplitude (Fig. 5d). Mele *et al.*[35] proposed a modified Maier–Göritz model[23] where they were able to fit the E'' value satisfactorily. A new variable designated as 'a' was introduced into the original Maier–Göritz model[23] to get the following expression which is known as the modified Maier–Göritz model:[23]

$$E''(\gamma) = E''_{st} + E''_{i}\frac{ac\gamma}{(1+c\gamma)^2} \quad (14)$$

This variable 'a' can be considered as a sensibility probe for the variations of the dissipative part E'' as a function of γ. Neither the Maier–Göritz model nor the modified Maier–Göritz model can properly fit the experimental values of E'', especially at low EMT content (Fig. 5d). Fitting parameters are tabulated in Table S4 and Table S5 in the ESI.†

3.4.1 Mechanical percolation behavior. We examine the occurrence of mechanical percolation behavior in NR–EMT nanocomposites by employing the Huber–Vilgis approach.[24]

The excess modulus (e) will be defined as

$$e = \frac{E' - E'_{\mathrm{m}}}{E_{\mathrm{m}}} \tag{15}$$

where E' is the dynamic storage modulus of the filled rubber at low amplitude and E'_{m} is the dynamic storage modulus of the unfilled rubber matrix at low amplitude.

Briefly, the excess modulus (e) of filled rubbers as a function of filler loading can be expressed as

$$e \sim \begin{cases} \varphi^n & \text{when } \varphi > \varphi_{\mathrm{p}} \\ \varphi & \text{when } \varphi < \varphi_{\mathrm{p}} \end{cases}$$

where the exponent $n = 1$ for filler volume fractions below the percolation threshold φ_{p}. This is in accordance with the Einstein–Smallwood equation for the hydrodynamic reinforcement of perfectly spherical filler particles and is valid for very small volume fractions. Above the percolation limit, a power law with $n > 1$ has been proposed for jammed systems.[36,37] The mechanical percolation threshold (φ_{p}) is obtained in a log–log plot where the experimental data are linearly interpolated according to the two different straight lines. It is observed from Fig. 6 that the φ_{p} of EMT particles is decreased when compared to OMT. This is attributed to the formation of a highly networked structure. Therefore, filler–filler networking can be formed even at very low loading of EMT particles. This conclusion is further supported by the observations from strain sweep measurements.

In the case of carbon black filled rubbers, Huber and Vilgis[24] derived the expression $n = 2/(3 - d_{\mathrm{f}})$ where d_{f} is the mass fractal dimension of the carbon black clusters (agglomerates), which are formed by aggregates as basic units. Furthermore, the Huber–Vilgis approach[24] gives a pre-factor $A = (R/b)^{\alpha}$ in $e = A\varphi^n$ where R is the mean cluster size and b is the mean diameter of the basic unit of carbon black agglomerates, *i.e.* the mean aggregate size. The exponent $\alpha = 2d_{\mathrm{f}}/(D - d_{\mathrm{f}})$ depends additionally on the spectral dimension D of the fractal clusters, *i.e.* from the measure of cluster connectivity.[27] In the case of modeling of carbon black agglomerates by diffusion-limited aggregation (DLA) clusters[38,39] with $d_{\mathrm{f}} \sim 2.5$ and $D \sim 4/3$, one finds $\alpha = 5/4$ and the Huber–Vilgis exponent $n = 4$. This means a strong deviation from a linear φ-dependence at large volume fractions $\varphi > \varphi_{\mathrm{p}}$. Although the Huber–Vilgis approach is only qualitative, we do arrive at some interesting conclusions. In the limiting case of compact filler particles ($d_{\mathrm{f}} = 3$), the overlap condition of the Huber–Vilgis[24] model would be hard to meet. With fractal dimensions (d_{f}) even slightly larger than 2.5, a drastic increase of the exponent would be observed, *i.e.* $n > 4$. Obviously, anisotropic clay filler particles lead to the opposite behavior as seen in Fig. 6.

In the case of OMT, we find that $n = 1.6$. Naively applying the Huber–Vilgis approach leads to a fractal dimension of $d_{\mathrm{f}} \approx 1.75$. Such clusters are less compact than DLA. A suitable visualization for it would be the cluster–cluster model (CCA)[33] with $d_{\mathrm{f}} = 1.78$ in 3 (Euclidean) dimensions. In CCA, one starts with a low concentration of particles diffusing on a lattice. When two particles meet, they form a cluster of two, which can also diffuse. When this cluster meets another two particles or another cluster, a larger cluster is formed. In the case of EMT in the rubber matrix (Fig. 6b), we find further reduction of compactness of the filler clusters (which may be attributed to the shaded diffuse spatial regions observed in the TEM micrograph). The slope $n \sim 0.7$ for EMT approaches a nearly vanishing fractal dimension $d_{\mathrm{f}} \sim 0.1$ which indicates less or even vanishing compactness of filler clusters. Note that even negative fractal dimensions have been introduced to help understand self-similar fractal measures called multifractals.[40]

We note that from the work of Pötschke *et al.*[41] corresponding scaling exponents for the equilibrium shear modulus as a function of volume fraction in polycarbonate nanocomposites filled with carbon nanotubes (CNT) can be calculated: $G_{\mathrm{e}} \sim \varphi^m$ with $m = 0.3$ and $m = 2.0$. This relatively low value of the exponent is also an indication of low compactness of CNT filler clusters. This is a similar situation to our clay systems, and is in contrast to the highly compact filler clusters in carbon black filled polymers. Moreover, the great discrepancy between the two exponents for CNTs is mainly due to the nanotube properties, like purity, aspect ratio, single or multiwall, and their state of dispersion in the matrix.

We observe that the last discussion point above helps to better understand mechanical properties of rubber

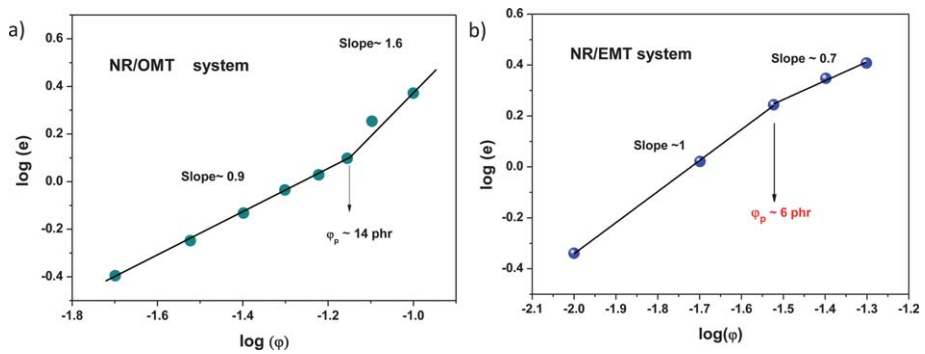

Fig. 6 Percolation threshold predicted from the Huber–Vilgis model: (a) NR–OMT system and (b) NR–EMT system.

nanocomposites within the context of common structural scaling models. However, these discussions should not be overstressed and considered as the last word on the subject. The fractal dimension of filler clusters in rubbers is sensitive to the surface modifications of filler particles as has been shown for silica (see, for example, the comprehensive discussion in ref. 42). This aspect has been excluded from our discussion here.

3.4.2 Frequency sweep and viscoelastic master curves. The master curve shows the dynamic mechanical behavior of the material over a very wide frequency range. The master curves for E' and E'' of NR gum and various NR–EMT blends with different clay loadings are shown in Fig. 7.

At high frequencies, the qualitative behavior of both E' and E'' is basically constant. However, the low frequency dependence of the moduli gradually changes for nanocomposites with 6 and 10 phr EMT. This observation may be attributed to the solid-like behavior of the nanocomposites beyond a certain volume fraction of EMT. Chung *et al.*[43] have also reported the same frequency dependence for NBR-layered silicate nanocomposites.

In general, a reference temperature (T_0) must be selected (in this case 20 °C) and the viscoelastic parameters at other temperatures are shifted to the corresponding values at that particular reference temperature. A horizontal shift factor, a_T, which is a function of temperature, enables one to obtain the master curves. The shift factor plots of various NR nanocomposites are documented in Fig. 8a. The Williams–Landel–Ferry (WLF) equation[44] (given below) is used to model the time–temperature behavior of all NR–EMT nanocomposites.

$$\log a_T = \frac{-C_1(T - T_0)}{C_2 + (T - T_0)} \tag{16}$$

where C_1 and C_2 are the WLF constants, T_0 is the reference temperature and T is the measurement temperature. Values of C_1 and C_2 obtained after fitting with the WLF equation for various NR–EMT nanocomposites are tabulated in Table 3. The values of C_1 and C_2 are related to the state of a material, in relation to its fractional free volume (f_0). Consequently, changes in f_0 are an indication of changes at the molecular level. The concept of free volume is difficult to define in a precise manner. In an approximate way we represent the segments of a polymer chain by rigid segments and the free volume as the "holes" present between those segments as a result of packing arrangements. Information on the dynamic free volume characteristics of the samples was deduced from the following equation:

$$C_1 = \frac{B}{2.303 f_0} \tag{17}$$

$$C_2 = \frac{f_0}{\alpha_f} \tag{18}$$

α_f is the coefficient of thermal expansion of the fractional free volume and B is a numerical constant, generally considered equal to unity. It is interesting to note that the values of C_1 and C_2 are increased after the addition of EMT compared to unfilled NR gum. Consequently, the fractional free volume (f_0) is also decreased which gives an indication of stronger rubber–filler interactions. In general, the value of f_0 reaches a constant value at T_g and increases linearly above T_g with the coefficient of thermal expansion (α_f). In the present investigation, the value of α_f is also decreased with increasing clay loading, which is summarized in Table 3. The mobility of the rubber chains is expected to be significantly reduced when adsorbed onto the clay surface compared to bulk unfilled rubber chains. The above observation is also supported from tan δ values obtained from DMA.

The temperature dependence of the a_T value, which is defined as the ratio of the relaxation time at a specified stress and the linear relaxation time at approximately zero stress level, is shown in Fig. 8a. There are numerous articles in the literature[45,46] stating that the a_T values are independent of the silicate loading. This suggests that the temperature dependent relaxation processes of nanocomposites observed in the dynamic mechanical measurements are unaltered even in the presence of the clay. However, the applicability of the principle of TTS for various NR–EMT nanocomposites indicates that the a_T values are mostly unchanged for up to 6 phr of clay loading. Beyond that there is a distinct change which is observed in a_T values. This change may be attributed to the higher degree of exfoliation of EMT particles throughout the rubber matrix.

Apparent activation energies (E_a) (a quantitative measure of the molecular mobility) can also be determined by substituting the WLF equation into the frequency shift factor in the Arrhenius equation, as follows:

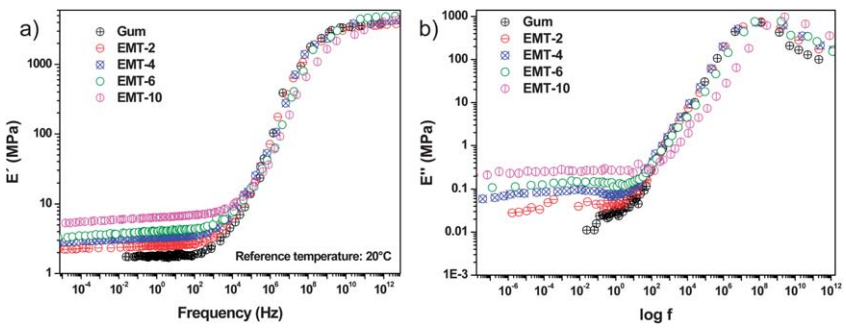

Fig. 7 Master curves generated by shifting (a) storage and (b) loss modulus curves according to the time–temperature superposition (TTS).

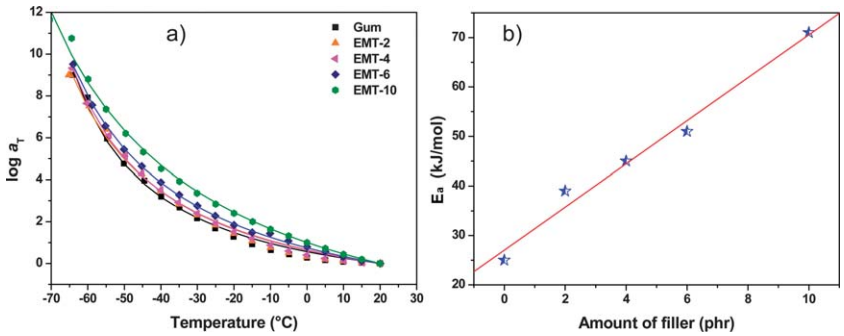

Fig. 8 (a) a_T values of NR and NR nanocomposites as a function of T. The line shown in the graph is the best fit WLF equation (eqn (16)) to the a_T values for all the NR–clay nanocomposites and the unfilled NR. (b) Apparent flow activation (E_a) energy as a function of EMT loading at 303 K.

Table 3 Viscoelastic parameters of different NR–clay nanocomposites

Sample	C_1	C_2	f_0	α_f (K^{-1})
Gum	2.5	106	0.173	1.63×10^{-3}
EMT-2	3.0	112	0.143	1.27×10^{-3}
EMT-4	3.5	114	0.124	1.08×10^{-3}
EMT-6	3.6	116	0.120	1.03×10^{-3}
EMT-10	6.0	126	0.076	5.75×10^{-4}
OMT-10	3.6	118	0.118	1.00×10^{-3}

$$E_a = R\left(\frac{\mathrm{d}\ln a_T}{\mathrm{d}(1/T)}\right) = 2.303R\left[\frac{C_1C_2T^2}{(C_2 + T - T_0)^2}\right] \quad (19)$$

Fig. 8b documents the EMT loading-dependent flow activation energy (E_{app}) of pure unfilled NR gum and various nanocomposites obtained from eqn (19). The apparent activation energy (E_{app}) of unfilled NR gum is 25.5 kJ mol^{-1}, and the E_{app} of the NR nanocomposites increases with the EMT loading to 31.2, 35.7, 37.1 and 53.7 kJ mol^{-1} for 2, 4, 6 and 10 phr of EMT, respectively. This behavior may be attributed to the improved dispersion distribution of EMT nanolayers in the NR matrix. Witten *et al.* also reported that trussing (or attachment) of the polymer chains onto the silicate surface may act as an energetic barrier to molecular motion.[47] The highest E_a value is obtained at 10 phr of EMT (compared to the same loading of OMT) (Table 4).

3.5 Swelling study: understanding the rubber–filler interactions

The extent of interaction between rubber and EMT is analyzed on the basis of an equilibrium swelling study. The volume fraction of rubber (V_r) in the swollen vulcanizates has a direct relationship with the crosslink density. In particular, the higher the value of V_r, the higher the reinforcing ability of the filler.

The Lorenz–Parks model[48] has been used for the investigation of the swelling of filler-reinforced vulcanizates which is given in eqn (20):

$$\frac{Q_f}{Q_g} = ae^{-z} + b \quad (20)$$

where Q is the amount of solvent per unit weight of the rubber, f and g refer to filled and gum blends respectively, z is the weight fraction of the filler in the polymer, and a and b are two constants which depend on the filler activity. In its current form this model has a drawback because it addresses the swelling behavior of a filled sample without acknowledging that the presence of a filler would enhance the crosslinking efficiency of the curing agent. Therefore, in the present study, the Cunneen–Russell equation[49] has been utilized. It represents a variant of the originally derived Lorenz–Parks equation and it is given by

$$\frac{V_{r0}}{V_{rf}} = ae^{-z} + b \quad (21)$$

where V_{r0} and V_{rf} are the volume fractions of the rubber in unfilled and filled vulcanizates, respectively, swollen in a solvent.

The ratio of V_{r0} to V_{rf} is a measure of rubber–filler interactions in filled systems. The values of a and b are calculated from the plot shown in Fig. 9a. A combination of higher values of a with lower values of b indicates strong rubber–filler interactions. Note that this combination is met in the case of NR–EMT system (when compared to NR–OMT).

Fig. 9b shows the plot of V_{r0}/V_{rf} against $\varphi/(1-\varphi)$ according to Kraus equation[50] given below:

$$\frac{V_{r0}}{V_{rf}} = 1 - \frac{m\varphi}{(1-\varphi)} \quad (22)$$

where

$$m = 3C(1 - V_{r0}^{0.3}) + V_{r0} - 1 \quad (23)$$

Table 4 E_a as a function of EMT loading and temperature (T)

	Temperature (K)				
Sample	213 K	223 K	232 K	263 K	303 K
EMT-2	285	181	133	66	39
EMT-4	299	196	142	74	45
EMT-6	308	208	153	83	51
EMT-10	310	229	250	108	71
OMT-10	255	175	134	72	45

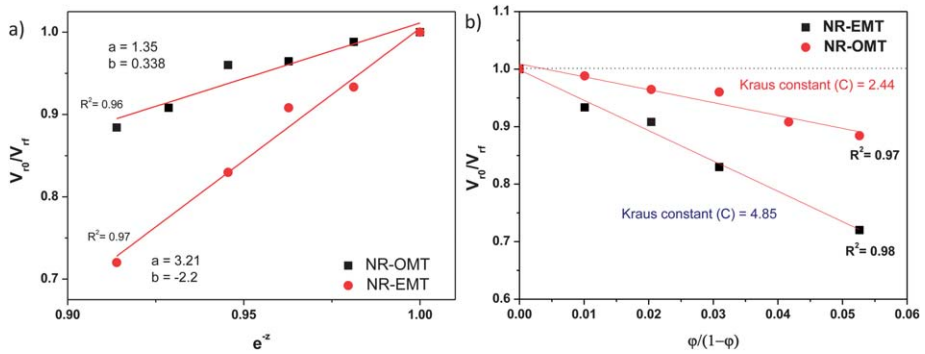

Fig. 9 (a) Cunneen–Russell plot. (b) Kraus plot of different NR–clay nanocomposites.

Here C is the characteristic constant for the filler, which is independent of solvent. φ is the volume fraction of the filler in the vulcanizate, and m represents the polymer–filler interaction parameter obtained from the slope of the plot of V_{r0}/V_{rf} against $\varphi/(1-\varphi)$.

The higher value of m observed for NR–EMT nanocomposites is attributed to their higher reinforcing ability compared to the NR–OMT system. The interaction parameter for EMT is found to be 4.85 as opposed to 2.24 for OMT.

4 Concluding remarks

Natural rubber (NR) nanocomposites containing highly exfoliated clay were prepared successfully utilizing the so-called 'propping-open approach'. Exfoliation of EMT particles in the NR matrix was observed by TEM. Guth–Smallwood and Halpin–Tsai models have been utilized to understand the reinforcement behavior of the rubber nanocomposites. The mechanical percolation threshold of EMT particles was decreased compared to OMT particles. This is attributed to the formation of a highly networked structure. Therefore, filler–filler networking can occur even at very low loading of EMT particles. This novel percolation phenomenon was further understood in terms of the mass fractal dimension of the nanoparticle clusters. A vanishing fractal dimension of the EMT clusters was observed. Non-linear viscoelastic behavior (Payne effect) was observed (even at 4 phr of EMT content) and was found to increase strongly with increasing amount of EMT. This further supports the idea of development of a highly networked filler structure. The molecular mobility of the macromolecular rubber chains was calculated and reported in terms of apparent activation energy. Higher activation energy was obtained in the case of NR nanocomposites with 10 phr EMT content. Finally, a higher value of the Kraus parameter m further supported the enhanced rubber–filler interaction especially in the case of EMT. The above observations are discussed in a mostly qualitative way by considering currently available empirical models. The results do form a clear picture that helps us to understand the underlying mechanism of rubber reinforcement, especially when the fillers are non-conventional with high aspect ratios.

Acknowledgements

The authors thank U. Reuter of Leibniz-Institut für Polymerforschung Dresden e.V. for TEM analysis.

References

1 E. Ruiz-Hitzky, M. Darder and P. Aranda, *J. Mater. Chem.*, 2005, **15**, 3650–3662.
2 P. L. Teh, Z. A. Mohd Ishak, A. S. Hashim, J. Karger-Kocsis and U. S. Ishiaku, *Eur. Polym. J.*, 2004, **40**, 2513–2521.
3 M. Arroyo, M. A. Lopez-Manchado, J. L. Valentin and J. Carretero, *Compos. Sci. Technol.*, 2007, **67**, 1330–1339.
4 S. Rooj, A. Das, K. W. Stöckelhuber, U. Reuter and G. Heinrich, *Macromol. Mater. Eng.*, 2012, **297**, 369–383.
5 S. Rooj, A. Das, K. W. Stöckelhuber, N. Mukhopadhyay, A. R. Bhattacharyya, D. Jehnichen and G. Heinrich, *Appl. Clay Sci.*, 2012, **67**, 50–56.
6 G. W. Brindley and S. Ray, *Am. Mineral.*, 1964, **49**, 106–115.
7 A. Usuki, Y. Kojima, M. Kawasumi, A. Okada, Y. Fukushima, T. Kurauchi and O. Kamigaito, *J. Mater. Res.*, 1993, **8**, 1179–1184.
8 Z. Changchun and L. J. Lee, *Macromolecules*, 2001, **34**, 4098–4103.
9 C. M. Koo, S. O. Kim and I. J. Chung, *Macromolecules*, 2003, **36**, 2748–2757.
10 A. Das, D.-Y. Wang, A. Leuteritz, K. Subramaniam, H. C. Greenwell, U. Wagenknecht and G. Heinrich, *J. Mater. Chem.*, 2011, **21**, 7194–7200.
11 J. Carretero-Gonzalez, H. Retsos, E. P. Giannelis, T. A. Ezquerra, M. Hernandez and M. A. Lopez-Manchado, *Soft Matter*, 2009, **5**, 3481.
12 M. J. Wang, *Rubber Chem. Technol.*, 1998, **71**, 520–589.
13 R. Scotti, L. Wahba, M. Crippa, M. D'Arienzo, R. Donetti, N. Santod and F. Morazzoni, *Soft Matter*, 2012, **8**, 2131–2143.
14 J. L. Valentín, I. Mora-Barrantes, J. Carretero-González, M. A. López-Manchado, P. Sotta, D. R. Long and K. Saalwächter, *Macromolecules*, 2010, **43**, 334–346.
15 M. Klüppel, R. H. Schuster and G. Heinrich, *Rubber Chem. Technol.*, 1997, **70**, 243.
16 V. M. Litvinov, R. A. Orza, M. Klüppel, M. V. Duin and P. C. M. M. Magusin, *Macromolecules*, 2011, **44**, 4887–4900.

17 M. Qu, F. Deng, S. M. Kalkhoran, A. Gouldstone, A. Robisson and K. J. Van Vliet, *Soft Matter*, 2011, **7**, 1066–1077.
18 A. Papon, S. Merabia, L. Guy, F. Lequeux, H. Montes, P. Sotta and D. R. Long, *Macromolecules*, 2012, **45**, 2891–2904.
19 S. S. Sternstein and A. J. Zhu, *Macromolecules*, 2002, **35**, 7262–7273.
20 E. Guth and O. Gold, *Phys. Rev.*, 1938, **53**, 322–328.
21 J. C. Halpin and J. L. Kardos, *J. Appl. Phys.*, 1972, **43**, 2235–2241.
22 G. Kraus, *J. Appl. Polym. Sci.: Appl. Polym. Symp.*, 1984, **39**, 75–92.
23 P. G. Maier and D. Göritz, *Kautsch. Gummi Kunstst.*, 1996, **49**, 18–21.
24 G. Huber and T. A. Vilgis, *Kautsch. Gummi Kunstst.*, 1999, **52**, 102–107.
25 Y. Q. Li and H. Ishida, *Macromolecules*, 2005, **38**, 6513–6519.
26 M. Takayanagi, T. Ogata, M. Morikawa and T. Kai, *J. Macromol. Sci., Part B: Phys.*, 1980, **17**, 591–615.
27 T. A. Vilgis, G. Heinrich and M. Klüppel, *Reinforcement of Polymer Nano-composites: Theory, Experiments and Applications*, Cambridge University Press, 2009.
28 G. K. Batchelor and J. T. Green, *J. Fluid Mech.*, 1972, **56**, 401–427.
29 H. S. Chen and A. Acrivos, *Int. J. Solids Struct.*, 1978, **14**, 349–364.
30 Y.-P. Wu, Q.-X. Jia, D.-S. Yu and L.-Q. Zhang, *Polym. Test.*, 2004, **23**, 903–909.
31 D. W. Schafer and R. S. Justice, *Macromolecules*, 2007, **40**, 8502–8517.
32 T. D. Fornes and D. R. Paul, *Polymer*, 2003, **44**, 4993–5013.
33 G. Heinrich and M. Klüppel, *Adv. Polym. Sci.*, 2002, **160**, 1–44.
34 J. L. Leblanc, *Filled Polymers: Science and Industrial Applications*, CRC press, Taylor and Francis Group, 2009, ch. 4.
35 P. Mele, H. A. Coussy, S. M. Boisseau and A. Dufresne, *Biomacromolecules*, 2011, **12**, 1487–1493.
36 V. Trappe, V. Prasad, L. Cipelletti, P. N. Segre and D. A. Weitz, *Nature*, 2001, **411**, 772–775.
37 C. S. O'Hern, L. E. Silbert, A. J. Liu and S. R. Nagel, *Phys. Rev. E: Stat., Nonlinear, Soft Matter Phys.*, 2003, **68**, 011306.
38 M. Klüppel and G. Heinrich, *Rubber Chem. Technol.*, 1995, **68**, 623–651.
39 *Fractals and Disordered Systems*, ed. A. Bunde and S. Havlin, Springer Verlag, 1991.
40 B. B. Mandelbrot, *Physica A*, 1990, **163**, 306–315.
41 P. Pötschke, M. Abdel-Goad, I. Alig, S. Dudkin and D. Lellinger, *Polymer*, 2004, **45**, 8863–8870.
42 A. S. Sarvestani and E. Jabbari, Nonlinear Viscoelastic Behavior of Rubbery Bionanocomposites, in *Rubber Nanocomposites: Preparation, Properties and Applications*, ed. S. Thomas and R. Stephen, John Wiley & Sons (Asia) Pte Ltd, 2010, p. 331.
43 J. W. Chung, K. S. Oh and S.-Y. Kwak, *Macromol. Mater. Eng.*, 2007, **292**, 627–633.
44 J. D. Ferry, *Viscoelastic Properties of Polymers*, Wiley, New York, 1st edn, 1980, p. 264.
45 E. P. Giannelis, R. Krishnamoorti and E. Manias, *Adv. Polym. Sci.*, 1999, **138**, 107–147.
46 J. Ren, A. S. Silva and R. Krishnamoorti, *Macromolecules*, 2000, **33**, 3739–3746.
47 T. A. Witten, L. Leibler and P. Pincus, *Macromolecules*, 1990, **23**, 824–829.
48 O. Lorenz and C. R. Parks, *J. Polym. Sci.*, 1961, **50**, 299–305.
49 J. I. Cunneen and R. M. Russell, *J. Rubber Res. Inst. Malaya*, 1969, **22**, 300.
50 G. Kraus, *J. Appl. Polym. Sci.*, 1963, **7**, 861–871.

